Fahd A. Mohiyaddin[1,2] · **Franklin G. Curtis**[1,2] · **M. Nance Ericson**[1,3] · **Travis S. Humble**[1,2]

Simulation of Silicon Nanodevices at Cryogenic Temperatures for Quantum Computing

Abstract Cryogenic nanoscale semiconductor devices are crucial for a wide variety of applications. The accurate design of such devices involve solving their electrostatics from fundamental semiconductor equations at low temperatures. We employ COMSOL to model a prototype cryogenic nanostructure, that can be used to readout the spin of a single electron in silicon, for quantum computing applications. By achieving convergence down to 15 Kelvin (K), we provide a guideline of techniques that aid to enhance convergence at cryogenic temperatures. We further compare the device electrostatics at different temperatures, which aids us to estimate the accuracy with temperature.

1 Introduction

Electronic devices operating at cryogenic temperatures are critical for a range of applications including space satellites, medicine, fundamental physics research and quantum computing. It is well known that cryogenic semiconductor devices exhibit fast operation speeds, low power dissipation, small leakage currents, reduced noise and thermal degradation, when compared to their room temperature counterparts [1, 2]. Advances in materials, superconductivity, electronic integration, and cooling techniques have further reinforced the significance and applications of low temperature nanoscale devices [3–5].

Optimal realization of these emerging cryogenic circuits and systems requires modeling and simulation tools with suitable accuracy at cryogenic temperatures. Simulation of these devices requires numerically solving the fundamental semiconductor equations [6] at low temperature, and estimating vital electrostatic parameters such as electric fields, currents, conduction band energies and carrier densities. However, the numerical modeling of semiconductor devices at cryogenic temperatures poses significant convergence issues since several parameters, such as carrier density, scale exponentially at such temperatures. This leads to intermediate solutions with sharp discontinuities in the electric fields and carrier densities, thereby failing to converge.

We report on techniques to ease convergence and extend modeling to the case of silicon based devices at very low temperatures. We illustrate this with an example of a 3-dimensional prototype device which can be used to readout the spin state of a phosphorus electron in a silicon quantum computer. We specifically employ the Semiconductor Module of the COMSOL MultiPhysics Software [7], since it offers the combined advantage of flexibility and capability to solve for several independent physical equations and parameters self-consistently. With proper choices of the finite-element solver, equations, initial values for the electron density, and an efficient mesh, we achieve convergence down to 15 K for the nanostructure. Our results for this specific device also directly fit into a broader context of developing a computational workflow to accurately design silicon devices for quantum computing [8].

The remainder of the paper is organized as follows: in Section 2, we outline the details of the nanostructure

This manuscript has been authored by UT-Battelle, LLC, under Contract No. DE-AC0500OR22725 with the U.S. Department of Energy. The United States Government retains and the publisher, by accepting the article for publication, acknowledges that the United States Government retains a non-exclusive, paid-up, irrevocable, world-wide license to publish or reproduce the published form of this manuscript, or allow others to do so, for the United States Government purposes. The Department of Energy will provide public access to these results of federally sponsored research in accordance with the DOE Public Access Plan (http://energy.gov/downloads/doe-public-access-plan).

[1]Quantum Computing Institute
Oak Ridge National Laboratory
Oak Ridge, TN

[2]Computational Sciences and Engineering Division
Oak Ridge National Laboratory
Oak Ridge, TN

[3]Electrical and Electronics Systems Research Division
Oak Ridge National Laboratory
Oak Ridge, TN

E-mail: mohiyaddinfa@ornl.gov

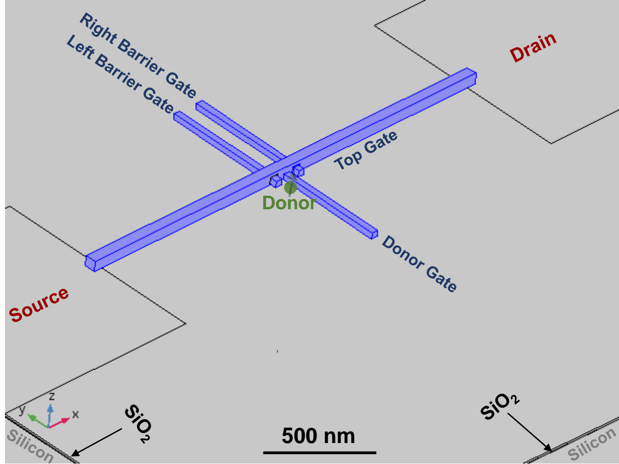

Fig. 1 COMSOL model of the MOS-based nanostructure employed in this work. The device can be used to readout the spin state of an electron bound to a phosphorus donor atom, which is implanted into the silicon substrate. Aluminum gate electrodes in the vicinity of the donor atom are highlighted in blue. The top, barrier and donor gate electrodes are biased at 1 V, 0 V and 0 V respectively.

used in this work. We then summarize the semiconductor equations solved by COMSOL, and highlight convergence issues at low temperature, in Section 3. Section 4 reviews the techniques that have aided in achieving convergence down to 15 K for this nanostructure. Section 5 describes the electrostatics observed in the device at 15 K. Finally in Section 6, we compare the results obtained at higher temperatures and quantify the accuracy of the simulations with temperature.

2 Test Nanostructure Model

The COMSOL model of the device is shown in Figure 1, and is comprised of a metal-oxide-semiconductor (MOS) silicon nanostructure with aluminum gate electrodes and SiO_2 dielectric. The top and barrier gate electrodes in Figure 1 are appropriately biased to create a single-electron-transistor (SET) at the Si-SiO_2 interface (shown later in Figure 4a) [9]. The source and drain regions correspond to heavily doped $n+$ regions having a phosphorus (^{31}P) concentration of 10^{20} cm^{-3}. Ohmic contacts are assigned to these regions with typical source-drain voltages (V_{DS}) $\sim$ 10 μV. The silicon substrate is lightly n doped with a ^{31}P concentration of 10^{13} cm^{-3}, and is grounded with an ohmic contact beneath it.

A ^{31}P donor atom is implanted next to the SET into the silicon substrate, as illustrated in Figure 1. Tuning the energy levels of the electron bound to the donor aids in reading out its spin state, and is elaborated later in Section 5 [10]. In a previous work, we showed that a semi-classical estimate of the conduction band energy is sufficient to estimate the donor electron energy and simulate spin-readout in such devices, to within a reasonable accuracy ($\sim$ 1 meV). We can also use the electrostatic potential and electric fields in the device as an input to a quantum-mechanical solver [11, 12], which in turn calculates precise donor energies and other parameters relevant to quantum computing [13].

To characterize the device electrostatics, including the electron density, conduction band energy and electric fields, we invoke the COMSOL Semiconductor module, which solves the semiconductor equations outlined in Section 3.

3 COMSOL Semiconductor Module at Low Temperature

Given an input device layout and gate voltages, the Semiconductor module solves the following Poisson and current continuity equations in the semiconductor, to estimate the carrier densities, currents and electrostatic potential [6, 7].

$$\nabla \cdot (\boldsymbol{\epsilon} \nabla V) = -q \left(p - n + N_{D^+} - N_{A^-} \right), \tag{1a}$$

$$\frac{\partial n}{\partial t} = \frac{1}{q} \left(\nabla \cdot \mathbf{J_n} \right) - U_n, \tag{1b}$$

$$\frac{\partial p}{\partial t} = -\frac{1}{q} \left(\nabla \cdot \mathbf{J_p} \right) - U_p, \tag{1c}$$

where $\boldsymbol{\epsilon}$ is the permittivity, V is the potential, q is the elementary charge, n and p are the electron and hole densities respectively, N_{D^+} and N_{A^-} are the ionized donor and acceptor densities respectively, t is the time, $\mathbf{J_n}$ and $\mathbf{J_p}$ are the electron and hole current densities respectively, and U_n and U_p are the net recombination rates for the electrons and holes respectively.

The carrier densities in Equation 1 are related to their quasi-Fermi energy levels, and the valence and conduction band energies, using the two well known equations below:

$$n = N_C \; F_{1/2} \left(\frac{E_{F_n} - E_c}{k_B T} \right), \tag{2a}$$

$$p = N_V \; F_{1/2} \left(\frac{E_v - E_{F_p}}{k_B T} \right), \tag{2b}$$

where N_C and N_V correspond to the density of states, $F_{1/2}(\eta)$ is the Fermi integral of order 1/2 and approaches e^{η} when $\eta \to -\infty$, E_c and E_v are the conduction and valence band edges respectively, E_{F_n} and E_{F_p} are the electron and hole quasi- Fermi levels respectively, k_B is Boltzmann constant, and T is the temperature. The band energies in Equations 2 are related to the electrostatic potential V, as follows:

$$E_c = -\chi - qV, \tag{3a}$$

Excerpt from the Proceedings of the 2017 COMSOL Conference in Boston

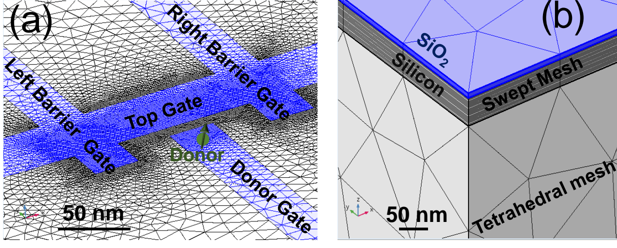

Fig. 2 (a) Mesh at the surface of the oxide, illustrating high mesh densities in the vicinity of gates. (b) Mesh at the corner of the device, highlighting a swept mesh in the oxide and in the substrate near the Si-SiO2 interface.

$$E_v = -\chi - E_g - qV, \tag{3b}$$

where χ is the electron affinity of silicon, and E_g is the band gap. Note that COMSOL considers the Fermi potential as the reference zero potential for V.

To calculate the charge densities arising from ionized donors, we employ the following incomplete ionization model:

$$N_{D^+} = \frac{N_D}{1 + g_D \exp\left(\frac{E_{F_n} - E_D}{k_B T}\right)}, \tag{4a}$$

$$N_{A^-} = \frac{N_A}{1 + g_A \exp\left(\frac{E_A - E_{F_p}}{k_B T}\right)}, \tag{4b}$$

where $E_{D(A)}$ and $N_{D(A)}$ are the impurity energy levels and doping densities respectively, $g_D = 2$ and $g_A = 4$ are the degeneracy factors of the impurities considering spin. Equations 2, 3 and 4 are fed into Equations 1a, 1b and 1c, which are self-consistently solved with appropriate boundary conditions over a finite mesh to estimate the n, p, V and their dependent variables in the semiconductor.

Voltages applied to the source, drain and substrate are modeled with an Ohmic boundary condition. This enforces charge neutrality for the electron and hole densities n_{eq} and p_{eq} respectively at the boundary, i.e.

$$n_{eq} - p_{eq} + N_a^- - N_d^+ = 0. \tag{5}$$

Substituting Equation 5 into Equations 2, 3 and 4, the Ohmic boundary condition yields

$$n_{eq} = \frac{1}{2}\left(N_d^+ - N_a^-\right) + \frac{1}{2}\sqrt{\left(N_d^+ - N_a^-\right)^2 + 4\gamma_n \gamma_p n_i^2}, \tag{6a}$$

$$p_{eq} = -\frac{1}{2}\left(N_d^+ - N_a^-\right) + \frac{1}{2}\sqrt{\left(N_d^+ - N_a^-\right)^2 + 4\gamma_n \gamma_p n_i^2}, \tag{6b}$$

$$V_{eq} = V_0 - \chi - \frac{E_g}{2q} + \frac{k_B T}{q}\left(\log\left(\frac{n_{eq}}{\gamma_n n_i}\right) + \frac{1}{2}\log\left(\frac{N_v}{N_c}\right)\right), \tag{6c}$$

where V_0 is the voltage applied at the Ohmic contact, V_{eq} is the electrostatic potential at the boundary, $n_i = \sqrt{N_c N_v}\exp\left(-E_g/2k_B T\right)$ is the intrinsic carrier density, and γ_n and γ_p are defined by the following:

$$\gamma_n = \frac{F_{1/2}\left(\frac{E_{F_n} - E_c}{k_B T}\right)}{\exp\left(\frac{E_{F_n} - E_c}{k_B T}\right)}, \tag{7a}$$

$$\gamma_p = \frac{F_{1/2}\left(\frac{E_v - E_{F_p}}{k_B T}\right)}{\exp\left(\frac{E_v - E_{F_p}}{k_B T}\right)}. \tag{7b}$$

All of the equations shown above are solved by COMSOL in the silicon substrate. The Poisson equation is solved to obtain electrostatics in the remainder of the device. Since the oxide and silicon substrate have different sets of equations that need to be solved, we ensure that the oxide and immediate substrate beneath it have the same lateral mesh. A tetrahedral mesh is then used for the remaining substrate. Figure 2 illustrates the mesh used for this nanostructure.

Note that the carrier densities n and p in Equation 2 have an exponential dependence on temperature. Assuming $E_c > E_F$, Figure 3a plots the spatial gradient of the logarithm of electron density n, as a function of electric field and temperature. For sufficiently low temperatures and large electric fields, we note that the electron densities vary sharply with position. For example, the electron density varies by over 2 orders of magnitude per nm, when the electric field approaches ~ 5 MV/m at 15 K. This hampers convergence as extremely fine meshes are required to capture the steep exponential gradients of the carrier densities at such temperatures. We also highlight that extremely small carrier densities at low temperatures cannot be calculated with the numerical precision available in COMSOL. This will lead to divide-by-zero errors, such as in Equation 6c. Figure 3b shows the COMSOL convergence plots at different temperatures, when the carrier densities are directly solved for, using the finite element method. The plot clearly indicates that obtaining convergence at temperatures below 50 K is challenging, and requires additional constraints and methods.

4 Guidelines for low temperature convergence

The nanostructure employed in this work is purely n-doped, and we are primarily interested in the electron densities, along with the potential. Hence, we first simplify the model and approximate the hole densities as $p = n_i^2/n$. This eases convergence by reducing the number of degrees of freedom (~ 1.5 million) to be solved. This approximation has negligible effect on the potential, electric fields and electron densities.

The source-drain voltage V_{DS} is 10 μV, which implies that the Fermi level E_F varies by 10 μeV in the

Excerpt from the Proceedings of the 2017 COMSOL Conference in Boston

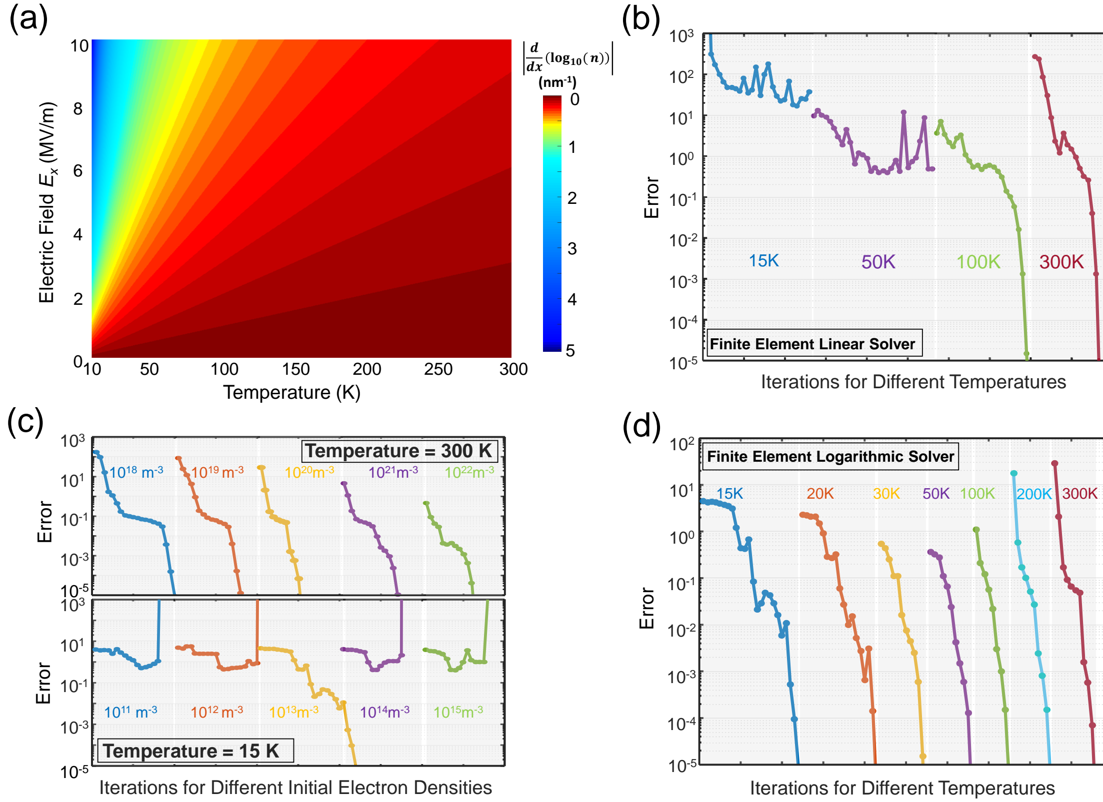

Fig. 3 (a) Spatial gradient of the logarithm of the electron density n as a function of electric field and temperature. At low temperatures and large electric fields, sharp gradients in n hamper convergence. (b)-(d) COMSOL convergence plots obtained for (b) different temperatures, when the finite-element method is used for solving the carrier density directly, (c) different initial starting values n_{init} of the electron density, at 300 K and 15 K, and (d) different temperatures by following the guidelines presented in Section 4. Each point in the convergence plots represents a single Newton iteration.

device. The variation of E_F causes significant convergence issues at low temperatures. Since, we are interested in the device potential, rather than currents, we approximate V_{DS} as 0 V. This condition limits the accuracy of the potential and conduction band energy (E_c) to within tens of μeV. We will see in Figure 4c that E_c varies by several meV in such devices, and that the above approximation is reasonable.

While the sharp exponential variation in the electron density hampers convergence, we can circumvent the issue by solving for the logarithm of the electron density n directly. This is implemented in the COMSOL Semiconductor module and results in better convergence at low temperatures, as the spatial variation of $\log(n)$ is more gradual than that of n.

By default, COMSOL uses the intrinsic carrier density (n_i) as an initial starting value (n_{init}) for the electron density while solving the semiconductor equations. n_{init} sets the scaling factors in the Jacobian matrix. At ultra low temperatures, n_i apporoaches zero, resulting in extreme values in the Jacobian, hampering convergence. Hence, it is crucial to choose an appropriate value of n_{init} at low temperatures. Figure 3c shows the COMSOL convergence plots for different n_{init}, at 300 K and 15 K. While different choices of n_{init} have negligible effect on convergence at 300 K, we highlight that even an order of magnitude deviation in n_{init} results in failed convergence at 15 K.

In Equation 6, V_{eq} varies logarithmically with the intrinsic carrier density n_i, which in turn has an exponential dependence on the temperature. The expression for V_{eq} can therefore be simplified to Equation 8 to yield the same physical equation, promoting smoother convergence. We note that this modification is critical when modeling the device below 25 K.

$$V_{eq} = V_0 - \chi + \frac{k_B T}{q}\left(\log\left(\frac{n_{eq}}{\gamma_n N_c}\right)\right). \qquad (8)$$

By following the above steps, we achieve convergence for temperatures down to 15 K, as illustrated in the convergence plots in Figure 3d. We can potentially obtain convergence at lower temperatures with auxiliary temperature sweeps, where the solution at each temperature step acts as an initial guess for the subsequent step. However, since the electron density varies significantly between subsequent steps, this technique has only aided us to further reduce the temperature by $\sim$ 3 K.

Excerpt from the Proceedings of the 2017 COMSOL Conference in Boston

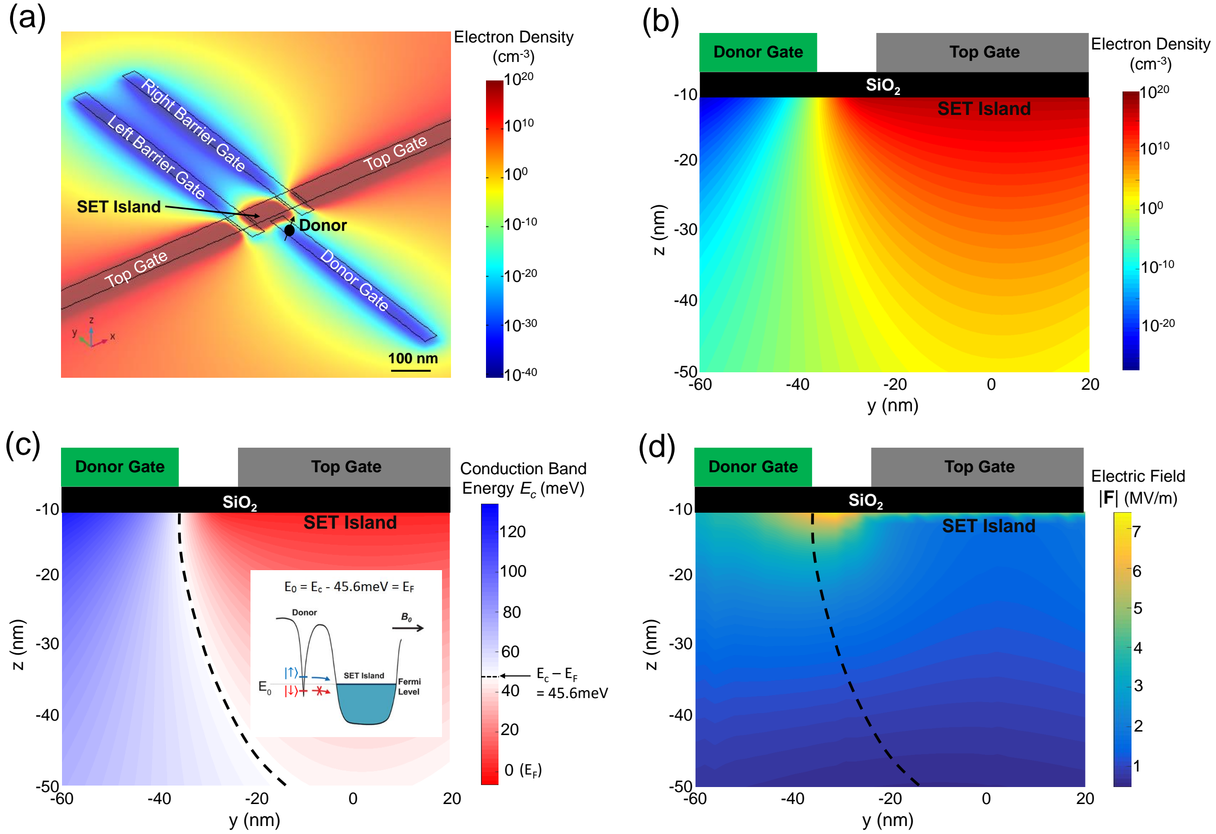

Fig. 4 (a) Electron density (n) in the device highlighting the single-electron-transistor (SET) island. (b) Electron density along an x-slice cut through the centre of the SET island. (c) Conduction band energy (E_c) variation illustrating the locations (dashed line) where the donor electron has the appropriate energy for its spin to be read out. Inset : Spin readout principle showing that the donor electron can preferentially tunnel to the SET island depending on its spin. (d) Magnitude of the electric field ($|\mathbf{F}|$) along the x-slice. All the above electrostatic parameters have been estimated with the Semiconductor Module in COMSOL.

Simplifications of the Fermi integral in Equation 2, and truncating extremely low carrier densities to finite values, may also aid in convergence at lower temperatures. This has been illustrated in previous works [14] and with other software [15]. We are yet to quantify the accuracy obtained with such techniques in COMSOL, and leave this for future work.

5 Device Electrostatics at 15K

We will now analyze the electrostatics in the device at 15 K. Figures 4a and 4b show the electron density (n) from the top and along a slice of the device respectively. The position of the single-electron-transistor (SET) island is evident in Figure 4a, where the barrier gates (biased at 0 V) completely diminish electrons beneath them. We also note that n varies by over 60 orders of magnitude from the SET island to the region under the donor and barrier gates. Such decays in the electron densities can be expected from Equation 2. However, at high electron density regions, we observed that n was fairly constant at 10^{20} cm^{-3} with temperature. This density is primarily determined by the gate potential, band bending at the interface and screening from existing electrons in these regions, and temperature has a much smaller effect.

Recall that the nanostructure also includes phosphorus donors implanted near the SET island. The SET aids to readout the spin of the donor electron using the following mechanism. The potential seen by the donor electron, including the Coulomb potential of its nucleus, is shown in the inset of Figure 4c. For spin readout, the energy of the donor electron is aligned with the Fermi Level of the SET island. In an externally applied magnetic field $\mathbf{B_0}$, the Zeeman energy splitting between the spin states results in preferential tunneling of the spin-up electron to the island, which modifies the current passing through the SET [10].

In a previous work for such devices, we computed that the energy of the donor electron is 45.6 $\pm$ 1 meV beneath the conduction band energy E_c [16]. We therefore use E_c obtained from COMSOL to model the donor electron energy to within an accuracy of $\sim$ 1 meV. Figure 4c plots E_c with respect to the Fermi level E_F, along a slice of the device. The dashed line

Excerpt from the Proceedings of the 2017 COMSOL Conference in Boston

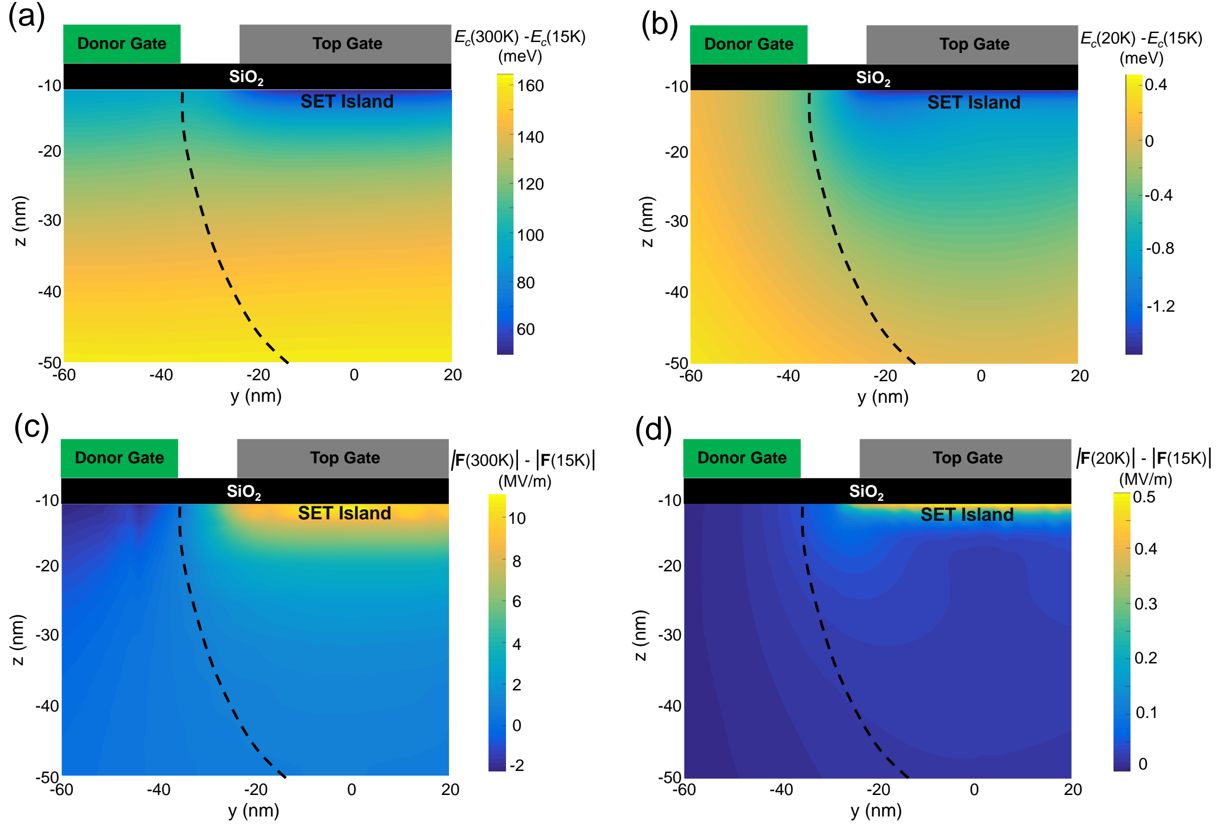

Fig. 5 (a)-(b) Difference between the conduction band energy E_c obtained with COMSOL at (a) 300 K and 15 K, and (b) 20 K and 15 K. (c)-(d) Difference between the magnitude of electric field $|\mathbf{F}|$ estimated at (c) 300 K and 15 K, and (d) 20 K and 15 K. The dashed line corresponds to spin-readout locations extracted from Figure 4c.

in Figure 4c shows locations where $E_c = 45.6$ meV. For the gate voltages used in the model, this line corresponds to positions where the donor electron has the appropriate energy ($\sim E_F$) for its spin to be read out.

Figure 4d shows the magnitude of the electric field $|\mathbf{F}|$ along a slice of the device. The electric fields of several MV/m in Figure 4d are indeed large enough to significantly modify parameters for quantum computing, such as hyperfine [17] and exchange couplings [18]. Finally, we emphasize that the magnitude and variation of the COMSOL electron densities, electric fields and conduction band energies are consistent with those from Sentaurus TCAD [15] on similar devices [16].

6 Comparison with Higher Temperatures

Quantum computing experiments performed on such devices are at milli-Kelvin (mK) temperatures. While we have only achieved convergence at temperatures far from the mK regime, comparison of results at higher temperatures can aid to quantify the accuracy of the simulations with temperature.

In Figure 5a, we plot the difference between the conduction band energies E_c obtained at 300 K and 15 K, and note significant discrepancies of $\sim$ 100 meV. The magnitude of the electric fields $|\mathbf{F}|$ are also different by several MV/m at the two temperatures, as indicated in Figure 5c. Hence, it is essential to simulate such devices at low enough temperatures.

Figures 5b and 5d plot the discrepancies of the conduction band energy and electric field, between 20 K and 15 K. The variation of both parameters with temperature are sensitive to the position. However, we emphasize that E_c and $|\mathbf{F}|$ differ by at most 0.5 meV and 0.1 MV/m respectively, at the spin readout locations estimated previously from Figure 4c. With E_c being $\sim$ 45.6 meV and the donor experiencing electric fields of several MV/m (Figure 4d), the spin readout locus will only be slightly different at the two temperatures, by well within a nm.

In Figure 6, we show the variation of E_c and $|\mathbf{F}|$ with temperature for different depths along the spin readout locus. For a range of temperatures between 15 K and 50 K, the plots indicate that the E_c and $|\mathbf{F}|$ will vary by less than 2 meV and 0.1 MV/m respectively, when the temperature is modified by 5 K. These would translate to inaccuracies of $\sim$ 1 nm in the spin readout locus, for temperature variations of 5 K.

Excerpt from the Proceedings of the 2017 COMSOL Conference in Boston

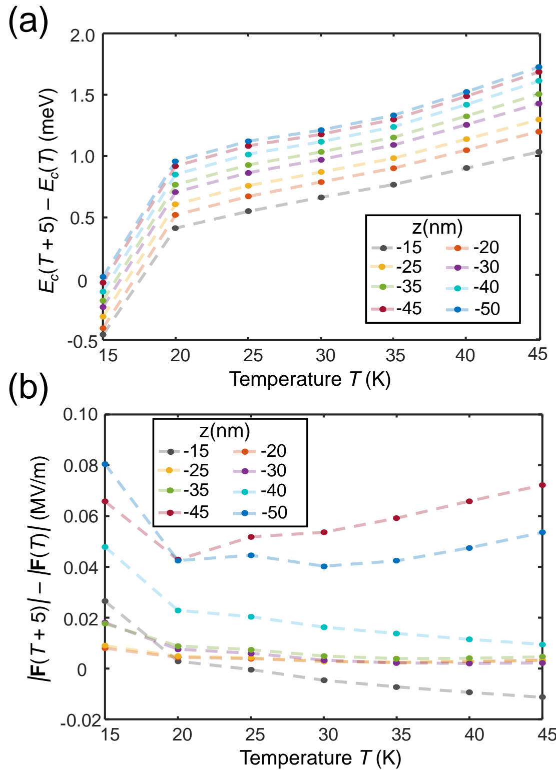

Fig. 6 Variation of (a) conduction band energy E_c, and (b) electric field $|\mathbf{F}|$ with temperature, obtained from COMSOL simulations. We specifically consider positions along the spin readout locus obtained from Figure 4c.

7 Summary

Electronic devices operating at low temperatures are becoming increasingly important in many modern applications in science and computing. Modeling and simulation of such devices at low temperatures is thereby critical for accurate device design and characterization. We have provided a guideline for simulating the electrostatics at low temperature with the COMSOL Semiconductor module, using an example of a silicon quantum computing device. We have analyzed the device electrostatics including the electron density, conduction band energy, electric fields and donor locations for spin readout at 15 K, and compared the results with higher temperatures. Future work will concentrate on obtaining convergence at lower temperatures (mK) using the additional techniques mentioned in Section 4, benchmarking COMSOL simulation results with measurements obtained from experimental devices, and also extending modeling to estimate currents and mobilities at low temperatures.

References

1. Gutierrez-D, E. A., Deen, J., and Claeys, C., *Low temperature electronics: physics, devices, circuits, and applications*, Academic Press, 2000.
2. Balestra, F. and Ghibaudo, G., "Physics and performance of nanoscale semiconductor devices at cryogenic temperatures," *Semiconductor Science and Technology*, Vol. 32, No. 2, Jan 2017, pp. 023002.
3. Balestra, F. and Ghibaudo, G., *Device and circuit cryogenic operation for low temperature electronics*, Springer Science & Business Media, 2013.
4. Deaver, J., Deaver, B. S., and Ruvalds, J., *Advances in superconductivity*, Springer Science & Business Media, 2013.
5. Cabrera, B., Gutfreund, H., and Kresin, V. Z., *From High-Temperature Superconductivity to Microminiature Refrigeration*, Springer Science & Business Media, 2012.
6. Sze, S. M. and Ng, K. K., *Physics of semiconductor devices*, John wiley & sons, 2006.
7. "Semiconductor Module User's Guide," COMSOL Multiphysics® v. 5.2a, COMSOL AB, Stockholm, Sweden, 2016.
8. Humble, T. S., Ericson, M. N., Jakowski, J., Huang, J., Britton, C., Curtis, F. G., Dumitrescu, E. F., Mohiyaddin, F. A., and Sumpter, B. G., "A computational workflow for designing silicon donor qubits," *Nanotechnology*, Vol. 27, No. 42, Sep 2016, pp. 424002.
9. Angus, S., Ferguson, A., Dzurak, A., and Clark, R., "Gate-Defined Quantum Dots in Intrinsic Silicon," *Nano Letters*, Vol. 7, No. 7, Jun 2007, pp. 2051–2055.
10. Morello, A., Pla, J., Zwanenburg, F., Chan, K., Tan, K., Huebl, H., Möttönen, M., Nugroho, C., Yang, C., van Donkelaar, J., et al., "Single-shot readout of an electron spin in silicon," *Nature*, Vol. 467, No. 7316, Oct 2010, pp. 687–691.
11. Klimeck, G., Ahmed, S. S., Bae, H., Kharche, N., Rahman, R., Clark, S., Haley, B., Lee, S., Naumov, M., Ryu, H., Saied, F., Prada, M., Korkusinski, M., and Boykin, T. B., "Atomistic simulation of realistically sized nanodevices using NEMO 3-D - Part I: Models and benchmarks," *IEEE Trans. Electron Devices*, Vol. 54, No. 9, Sep 2007, pp. 2079–2089.
12. Klimeck, G., Ahmed, S. S., Kharche, N., Korkusinski, M., Usman, M., Prada, M., and Boykin, T. B., "Atomistic simulation of realistically sized nanodevices using NEMO 3-D - Part II: Applications," *IEEE Trans. Electron Devices*, Vol. 54, No. 9, Sep 2007, pp. 2090 – 2099.
13. Zwanenburg, F. A., Dzurak, A. S., Morello, A., Simmons, M. Y., Hollenberg, L. C. L., Klimeck, G., Rogge, S., Coppersmith, S. N., and Eriksson, M. A., "Silicon quantum electronics," *Reviews of Modern Physics*, Vol. 85, No. 3, Jul 2013, pp. 961–1019.
14. Nielsen, E., Gao, X., Kalashnikova, I., Muller, R. P., Salinger, A. G., and Young, R. W., "QCAD simulation and optimization of semiconductor double quantum dots," Tech. rep., Sandia National Laboratories, 2013.
15. "Sentaurus Device User Guide," Synopsys ® v. J-2014.09, Synopsys Inc., Mountain View, California, United States of America, 2014.
16. Mohiyaddin, F. A., Rahman, R., Kalra, R., Klimeck, G., Hollenberg, L. C. L., Pla, J. J., Dzurak, A. S., and Morello, A., "Noninvasive Spatial Metrology of Single-Atom Devices," *Nano Lett.*, Vol. 13, No. 5, May 2013, pp. 1903–1909.
17. Rahman, R., Wellard, C., Bradbury, F., Prada, M., Cole, J., Klimeck, G., and Hollenberg, L., "High Precision Quantum Control of Single Donor Spins in Silicon," *Phys. Rev. Lett.*, Vol. 99, Jul 2007, pp. 036403.
18. Wellard, C. J., Hollenberg, L. C. L., Parisoli, F., Kettle, L. M., Goan, H.-S., McIntosh, J. A. L., and Jamieson, D. N., "Electron exchange coupling for single-donor solid-state spin qubits," *Phys. Rev. B*, Vol. 68, Nov 2003, pp. 195209.

Excerpt from the Proceedings of the 2017 COMSOL Conference in Boston